Very old firn air linked to strong density layering at Styx Glacier, coastal Victoria Land, East Antarctica

Youngjoon Jang[1], Sang Bum Hong[2], Christo Buizert[3], Hun-Gyu Lee[1], Sang-young Han[1], Ji-Woong Yang[1], Yoshinori Iizuka[4], Akira Hori[5], Yeongcheol Han[2], Seong Joon Jun[2], Pieter Tans[6], Taejin Choi[2], Seong-Joong Kim[2], Soon Do Hur[2], and Jinho Ahn[1*]

[1]School of Earth and Environmental Sciences, Seoul National University, Seoul, Republic of Korea

[2]Korea Polar Research Institute, Incheon, Republic of Korea

[3]College of Earth, Ocean, and Atmospheric Sciences, Oregon State University, Corvallis, Oregon, USA

[4]Institute of Low Temperature Science, Hokkaido University, Sapporo, Japan

[5]Kitami Institute of Technology, Kitami, Japan

[6]National Oceanic and Atmospheric Administration, Earth System Research Laboratory, Boulder, CO, USA

Corresponding to: Jinho Ahn (jinhoahn@gmail.com)

Abstract

Firn air provides plenty of old air from the near past, and can therefore be useful for understanding human impact on the recent history of the atmospheric composition. Most of the existing firn air records cover only the last several decades (typically 40 to 55 years) and are insufficient to understand the early part of anthropogenic impacts on atmosphere. In contrast, a few firn air records from inland sites, where temperatures and snow accumulation rates are very low, go back in time about a century. In this study, we report an unusually old firn air effective CO_2 age of 93 years from Styx Glacier, near the Ross Sea coast in Antarctica. This is the first report of such an old firn air age (> 55 years) from a warm coastal site. The lock-in zone thickness of 12.4 m is larger than at other sites where snow accumulation rates and air temperature are similar. High-resolution X-ray density measurements demonstrate a high variability of the vertical snow density at Styx Glacier. The CH_4 mole fraction and total air content of the closed pores also indicate large variations in cm-scale depth intervals, indicative of layering. We hypothesize that the large density variations in the firn increase the thickness of the lock-in zone and, consequently, increase the firn air ages because the age of firn air increases more rapidly with depth in the

lock-in zone than in the diffusive zone. Our study demonstrates that all else being equal, sites where weather conditions are favourable for the formation of large density variations at the lock-in zone preserve older air within their open porosity, making them ideal places for firn air sampling.

1 Introduction

Bubbles trapped in ice cores preserve ancient air and allow direct measurements of the atmospheric composition in the past (e.g., Petit et al., 1999). However, it is difficult to obtain air samples over the past several decades from ice cores since the more recent air has not yet been completely captured into bubbles closed off from the atmosphere. In contrast, we can obtain the recent records from the interstitial air in the porous, unconsolidated snow layer (firn) on top of glaciers and ice sheets (Schwander et al., 1989, 1993). In addition, we can take advantage of the very large amount of firn air because it allows us to accurately analyze isotopic ratios of greenhouse gases and many trace gases such as man-made CFCs, HCFCs and SF_6 (Buizert et al., 2012a; Laube et al., 2012). However, reported firn air ages date back only several decades at the sites where snow accumulation rates are relatively high (Table 1). Old firn air (> 55 years) was observed only at sites where surface temperatures and snow accumulation rates are low such as South Pole (Battle et al., 1996) and inland Antarctic Megadunes (Severinghaus et al., 2010) (Table 1); however, even under such circumstances very old firn air is not guaranteed, as demonstrated by Dome C (Table 1).

In the firn layer, air moves through the open pores and is occluded into the adjacent ice at at total porosity of ~0.1 (Schaller et al., 2017). Firn air moves downward with the adjacent ice (advection), but is furthermore mixed by diffusion, and affected by thermal and gravitational fractionation (Craig et al., 1988; Johnsen et al., 2000; Severinghaus et al., 2001; Goujon et al., 2003). In addition, the gradual bubble trapping in the firn affects the movement of the air. As a result, at each depth there is a gas age distribution (Schwander et al. 1993; Trudinger et al., 1997), rather than a single gas age. Therefore, studying firn air is also important for interpreting the record of ancient air trapped in ice cores.

The firn column is generally divided into three zones: convective, diffusive and lock-in, depending on the mechanisms of firn air movement (Sowers et al., 1992). The gravitational enrichment in ^{15}N of N_2 is traditionally used to define the boundaries between these zones. The convective zone is the upper part of the firn where the air can ventilate with the overlying atmosphere. With stronger wind pumping, there can be a deeper convective

zone (Kawamura et al., 2013). This zone has the same $\delta^{15}N$ of N_2 value as that of the atmosphere. The diffusive zone is located under the convective zone, where molecular diffusion is the dominant mechanism of trace gas transport in interstitial air (Blunier and Schwander, 2000). The age of the firn air increases slowly with depth in the diffusive zone because of continued gas exchange with atmospheric air via diffusion. Heavier isotopes are enriched with depth due to the gravitational fractionation in the diffusive layer. Thus, $\delta^{15}N$ of N_2 gradually increases with depth in the diffusive zone. In the lock-in zone (LIZ) below the diffusive zone, gas diffusion is strongly impeded although the bubbles are not entirely closed. The top of the lock-in zone is called lock-in depth (LID), where the gravitational fractionation ceases, so that the $\delta^{15}N$ of N_2 becomes constant. The bottom of the LIZ is defined as the full close-off depth (z_{COD}), where all air bubbles are closed off and firn becomes sealed ice. The z_{COD} can be estimated in two different ways. First, we can calculate the z_{COD} from firn densification models. Typically, the close-off occurs when the density of ice reaches about 830 kg m^{-3} (Blunier and Schwander, 2000), equivalent to a critical porosity of around 0.1 (Schaller et al., 2017). Also, if temperature is known, the average density at close-off can be estimated from empirical relations (Martinerie et al., 1992). Second, the deepest position where air can be sampled from the firn column is commonly considered as (just above) the z_{COD}. In theory, the z_{COD} is the depth at which all pores are closed, but it can be ambiguous to specify the z_{COD} in the field because firn air can be sampled at a slightly deeper depth than that of the shallowest impermeable snow layer due to the existence of permeable layers at deeper depths – this effect is due to density layering (Mitchell et al., 2015).

The gas ages in the LIZ increase with depth faster than in the diffusive zone. In the LIZ, firn air moves downward at nearly the same rate as the surrounding ice, and therefore the age of the air increases with depth at nearly the same rate as the age of ice increases.

The age of the firn air is directly related to the movement of the firn air. Firn air models help calculate the firn air age using some parameters such as temperature and accumulation rate. However, several studies found that layering also affects the movement of firn air (e.g., Mitchell et al., 2015; Schaller et al., 2017). This implies that physical properties of the ice may affect the age of the firn air as well.

With regard to the lock-in and close-off processes, recent studies have focused on snow layers and microstructure of the firn (Hörhold et al., 2011; Gregory et al., 2014; Mitchell et al., 2015; Schaller et al., 2017). Density variability on millimeter to tens of cm scales is observed in all polar sites. Hörhold et al. (2011)

84 demonstrate that density variability is caused by physical snow properties in the firn column. Several studies
85 have dealt with how snow density variations affect the transport of firn air (Hörhold et al., 2011; Mitchell et al.,
86 2015). Mitchell et al. (2015) showed that the firn layering can affect the closure of pores and the thickness of
87 LIZ, but the relation between snow density variations and range of firn air ages was not quantitatively examined.
88 In this study, we present firn air composition and $\delta^{15}N\text{-}N_2$ from Styx Glacier, East Antarctica to better
89 understand the role of snow density variations on the age of firn air. We also present X-ray density data with
90 millimeter resolution and compare them with $\delta^{18}O_{ice}$ and the closed-pore air composition in the LIZ.
91 We hypothesize that large snow density variations make the LIZ thicker and facilitate preservation of old firn
92 air at the Styx Glacier. This study will help us better understand how the snow density layers of firn column
93 affects movement and preservation of firn air, and provide guidance on selecting good sites for future firn air
94 studies.
95
96 **2 Materials and Methods**
97 **2.1 Firn air sampling and gas mole fractions analysis**
98 The firn air and ice core were collected at the Styx Glacier, East Antarctica (73° 51.10' S, 163° 41.22' E, 1623
99 m asl) in December of 2014 (Fig. 1). This site is located 85 km north of the Korean Jang Bogo Station in the
100 Southern Cross Mountains near the Ross Sea (Han et al., 2015). The snow accumulation rate is ~10 cm ice year^{-1}
101 , calculated from the Styx16b ice chronology based on methane correlation and tephra age tie-point and
102 thinning functions (Yang et al., 2018). The mean annual surface temperature was measured as -31.7℃ by
103 borehole temperature logging at 15 m depth, two years after the ice core drilling (Yang et al., 2018). Table 1
104 lists the characteristics of the Styx Glacier and other firn air sampling sites. A total of 13 samples from the
105 surface to 64.8 m depth were collected. The firn air sampling device was constructed, following the design of
106 the University of Bern, Switzerland (Schwander et al., 1993). Three vacuum pumps (two diaphragm pumps and
107 one metal bellows pump), several pressure gauges, stainless steel lines, and vacuum valves were housed in an
108 aluminum case to transfer to the polar site. The pump system plays four major roles: (1) purging modern air
109 from the bottom of a borehole, (2) inflating the bladder to block the deep firn layers from the atmosphere, (3)
110 removing the contaminated air and extracting the firn air, (4) transporting firn air to a CO_2 analyzer for

measurements of gas mole fractions and store it in firn air containers. The bladder system is designed to be lowered into the borehole to seal the deep firn layer(s) being sampled from the atmosphere. The bladder consists of a 4 m-long rubber tube and metal caps on top and bottom of the rubber tube. The bladder's external diameter is 119.5 mm and internal diameter is 114.5 mm. The material of the tube is butyl rubber (BIIR) which can endure low temperatures, providing no risk of sample contamination.

The firn air samples were collected in 3-liter glass flasks at all collection depths. However, to test preservation ability of the sample air containers, Silcocan canisters were also used at 4 depths (0, 35.36, 43.42, 53.95 m). Accurate mole fractions of CO_2, CH_4, and SF_6 were measured at US National Oceanic and Atmospheric Administration (NOAA; https://www.esrl.noaa.gov/). The results for the two types of containers show good agreements. $\delta^{15}N$ of N_2 was analyzed at Scripps Institution of Oceanography for correcting gravitational fractionation effect (Severinghaus et al., 2010).

2.2 Firn air transport model

We used the Center for Ice and Climate (CIC) firn air model which is a 1-dimensional advection-diffusion model to simulate how the air moves in Styx firn column. In this model, there are four types of air transport in the open porosity: (1) molecular diffusion, (2) vigorous mixing in the convective zone, (3) advection, and (4) dispersion in the deep firn (Buizert, 2012b, Buizert and Severinghaus, 2016). The model uses the stochastic bubble trapping formulation described by Mitchell et al. (2015).

2.3 CH_4 in closed bubbles and total air content measurements

CH_4 mole fraction in the (closed) air bubbles in the firn was measured at Seoul National University using a melt-refreeze air extraction method (Yang et al., 2017). 124 discrete firn samples (cross section of 8.5 cm × 3 cm, length of 3 cm, ~35 g) were prepared from 4 different depth intervals in the lock-in zone (54.59-55.34, 58.11-59.05, 59.86-60.55, 64.02-65.25 m). All ice samples were cut and trimmed by ~2.5 mm with a band saw to remove contaminants on the surface ice. Then, the ice samples were inserted into the glass flasks attached to the gas extraction line. The pump system evacuated air in the flask placed in a cooled ethanol bath at -70 ℃ for 20 min. The evacuation time was limited to 20 minutes to prevent from gas loss due to pore openings by

sublimation. After the pressure dropped below 0.2 mTorr, the ice samples in the glass flask were melted and air in the bubbles was extracted. After the melting was finished, we refroze the ice using a cooled ethanol bath to release the gas dissolved in the ice melt. Finally, the extracted air was injected into the sample loop of the gas chromatograph equipped with a flame ionization detector (FID). The calibration curve of the GC-FID was calculated by the standard air prepared at NOAA with a CH_4 mole fraction of 895 ppb on the NOAA04 scale (Dlugokencky et al., 2005).

Total air content of the firn ice samples was analyzed simultaneously with CH_4 mole fraction using the wet extraction system at SNU. The total air content was expressed as the volume of air trapped in the closed pores of unit mass of firn ice sample (in unit of ml per gram ice at STP conditions). The volume of air extracted from a firn ice sample was calculated by the ideal gas law with the internal pressure, volume and temperatures of the sample flasks and vacuum lines. The pressure of extracted air was measured by a pressure manometer connected to the sample loop of the GC-FID. As no direct measure of temperature was available, the temperature of extracted air was assumed to be identical to the surrounding temperatures; the ethanol temperature was used for the sample flasks, room temperature for vacuum lines, and valve box temperature (50°C) for the sample loop. In this study, the corrections for bubble-cut effect and thermal gradient within vacuum line were not considered. More detailed description of the protocols of total air content measurements is described in Yang (2019).

2.4 Analysis for stable isotopes of ice

After completing the measurements of the CH_4 mole fraction in air, the melt water was put into cleaned 125 ml bottles and analyzed for water stable isotope ratios at Korea Polar Research Institute (KOPRI) using a Cavity Ring-Down Spectroscopy (CRDS, L1102-i, Picarro, USA) system. We performed the same analysis for the snow pit samples, but without CH_4 analysis. The data are here presented as δ-notations:

$$\delta^{18}O = (({}^{18}O/{}^{16}O)_{sample}/({}^{18}O/{}^{16}O)_{VSMOW} - 1) \quad (1)$$

The firn ice melt was filled into a 400 μl insert in a 2 ml glass vial using a syringe filter. The auto sampler transported the ice melt samples in the insert to the vaporizer about 180 nl at a time. The samples with the liquid state were transferred to the cavity after being converted into the water vapor in a vaporizer at 110 ℃. The measurement precision evaluated by measuring an in-house standard repeatedly (n=12) was 0.08‰ (1 sigma

166 standard deviation).

167

168 **2.5 X-ray firn density measurement**

169 We obtained high-resolution density data using the X-ray transmission method reported by Hori et al. (1999)
170 for the firn ice at various depth intervals. This method is advantageous because it can measure continuously and
171 non-destructively. The X-ray beam penetrates the ice samples and the detector on the opposite side analyzes the
172 intensity of the beam. To make equal thickness for each core section, upper and side parts of the half circle-
173 shape core were shaved by a microtome. After putting the precut ice core on a rack, we set the rate of
174 measurement at 50 mm min^{-1}, and finally obtained 1mm-resolution density data.

175

176 **3 Results**

177 **3.1 Layered stratigraphy**

178 We examined a snow pit, located 10 m away from the main ice core borehole, 2 years after drilling to
179 understand the physical properties such as layers, density, and ice grain size of the upper firn at Styx site. We
180 scratched the snow wall by hand to remove soft layers and enhance the visibility of hard layers (Fig. 2a). The
181 soft layers are presumed to be depth hoar, and the hard ones are wind crusts (Fig. 2b). The alternating layers
182 repeat with intervals of few centimeters to 20 centimeters. The top boundaries of the hard layers are sharp and
183 extend horizontally about a meter, but the bottom boundaries are not well defined due to gradual density changes.
184 10 cm-resolution density data were obtained by a density cutter (Proksch et al., 2016). The soft layers are coarse-
185 grained, while the hard ones are fine-grained (Fig. 2b-d).

186

187 **3.2 Firn gas sampling and the age of firn air**

188 We calibrate the depth-diffusivity profile in the model using trace gases with a well-known atmospheric
189 history (Buizert et al., 2012a; Trudinger et al., 2013; Witrant et al., 2012). The atmospheric time series from
190 well-dated firn air (MacFarling Meure et al., 2006) and instrument measurement records (NOAA;
191 https://www.esrl.noaa.gov/) were used for calibration. The simulated mole fraction profiles match well with the
192 observations (Fig. 3). CO_2, CH_4, SF_6 and $\delta^{15}N\text{-}N_2$ distributions in firn air were modeled. The model does not

include thermal fractionation, and therefore provides a poor fit to the $\delta^{15}N\text{-}N_2$ data in the upper firn where seasonal temperature gradients fractionate the gases. Fitting the barometric equation to the $\delta^{15}N$ data of the upper diffusive zone suggests a convective zone thickness of approximately 3 m. This is within the typical range of observed convective zones, but perhaps lower than expected for a very windy site (Kawamura et al. 2006). The firn air age (black curves in Fig. 3) slowly increases with depth at the diffusive zone because it mixes with fresh atmospheric air on the surface mostly by molecular diffusion (Blunier and Schwander, 2000). In contrast, the firn air age rapidly increases within the LIZ at a rate similar to that of the ice age. The gas age distribution of Styx ice at z_{COD} is narrower than the other sites where old firn air is reported (Fig. 4); we simulate a spectral width of 15.9, 22.8 and 45.5 years at Styx, South Pole, and Megadunes, respectively. This means that the past atmospheric history of trace gases can in principle be reconstructed with higher resolution at Styx than at the other old-air firn sites.

We estimate the age of samples in two ways. First, after calibrating the firn air model, we can derive the mean sample age from the simulated gas age distribution. At the deepest Styx sampling depth (64.8 m) we simulate a mean CO_2 age of 102 years, and a mean CH_4 age of 97 years; the CH_4 age is younger than the CO_2 age due to the higher diffusivity of CH_4. Second, we can estimate the sample ages by comparing the measured trace gas concentrations directly to the atmospheric histories of these gases – this age has been called the "effective age" (Trudinger et al. 2013). The lowest CO_2 mole fraction of 305.18 ppm at depth of 64.8 m (304 ppm after correcting for gravitational enrichment) corresponds to the year 1921 an effective age of 93 years (relative to sampling year 2014) on the Law Dome ice core record (MacFarling Meure et al., 2006; Rubino et al., 2019). The CH_4 mole fraction of 943.36 ppb at the same depth (946.5 after gravitational correction) corresponds to an effective age of 96 years (MacFarling Meure et al., 2006) (Figs. 3a, 3b).. The second method provides younger ages because the growth rate in the atmospheric mixing ratios of these gases has increased over time, biasing the effective ages towards younger values (Trudinger et al. 2002). Table 1 lists effective CO_2 ages in the deepest firn air sample for several sites; we here compare the effective CO_2 age between sites rather than the modeled mean age, as it is purely empirical and does not rely on model assumptions.

Only few firn air sites have effective CO_2 ages around 93 years or older: 91 years from the South Pole (Battle et al., 1996) and 129 years from Megadunes (Severinghaus et al., 2010; Table 1)**.** These sites are located in

interior Antarctica and have low annual mean temperatures and low snow accumulation rates (Table 1). Firn densification takes a long time if snow accumulation and/or temperature are low, therefore firn air can be preserved for a long time without being trapped. In contrast, the Styx site is located near the coast and has relatively high snowfall, and therefore the age of 93 years is very unusual. Sites of comparable climate characteristics typically have an oldest firn air age of around 40 years. This indicates that there may be other factors that can permit preservation of the old firn air at Styx Glacier.

3.3 Density layering and its influence on bubble trapping

Firn density is the primary control on the bubble close-off process. Density layering leads to staggered bubble trapping, with high-density layers closing off before low-density ones (Stauffer et al., 1985; Etheridge et al. 1992, Mitchell et al. 2015, Rhodes et al. 2016).

Because the mole fractions of atmospheric greenhouse gases (CO_2, CH_4, N_2O) have increased during the last century, we may obtain information on the timing of the closure of the bubbles from the greenhouse gas mole fractions of the air trapped in closed bubbles. In this study, we used the CH_4 concentration in closed bubbles ($[CH_4]_{cl}$) and the total air content of the firn ice as indicators of the close-off process. The density and $[CH_4]_{cl}$ show an anti-correlation (Fig. 5). Our results confirm the CH_4 concentration-total air content relation observed in West Antarctic Ice Sheet (WAIS) Divide firn ice (Mitchell et al., 2015). High-density layers reach the lock-in and close-off densities at shallower depths than low-density layers. Thus, air bubbles are trapped at shallower depths in high-density layers. Early trapped bubbles preserve older air with lower greenhouse gas mole fractions. Higher air content is expected in the high-density layers, in which open porosity is small and closed porosity is large (Fig. 5). However, we cannot entirely exclude the possibility of some post-coring bubble close-off (Aydin et al., 2010). High open porosity in low-density layers may have more chances to trap modern ice storage air, which has higher mole fraction of CH_4 than atmospheric background levels.

Figure 5a shows $[CH_4]_{cl}$ and total air content in the LIZ of the Styx firn. $[CH_4]_{cl}$ generally decreases with depth and the cm-scale variability is reduced in the deep layers, while the total air content generally increases with depth. The $[CH_4]_{cl}$ greater than CH_4 mole fraction in neighboring firn air (green line in Fig. 5a-d) indicates part of bubbles formed after coring and increased the $[CH_4]_{cl}$, as previous studies also observed (Mitchell et al.,

2015; Rhodes et al., 2013). Most of $[CH_4]_{cl}$ data show large cm-scale variations (Fig. 5). The highs and lows of $[CH_4]_{cl}$ repeat with cycles of 6 to 24 cm (Fig. 5e). Note that the layering observed in the snow pit likewise shows irregular intervals (Fig. 2b). From the layer spacing, we conclude that bubble trapping at Styx is not controlled by annual layers (Section 4), as was observed at Law Dome (Etheridge et al. 1992).

The evolution of CH_4 in the closed porosity may give information on how the snow layers can induce inhomogenous records and help constrain the gas age distribution in ice (Fourteau et al. 2017). However, the details are beyond the scope of this study and we will focus on the firn air age in the open porosity.

3.4 High-resolution firn density measurements

The X-ray measurements show highly variable density on cm scales. We converted the high-resolution density to total porosity using the following equation:

$$\Phi_{\text{total}} = 1 - \frac{\rho}{\rho_{\text{ice}}} \quad (2)$$

where ρ = density of porous ice; ρ_{ice} = density of bubble-free ice (919 kg m^{-3}); and Φ = porosity. We test the idea that the lock-in zone corresponds to the depth range bounded by the first closed layer (porosity below 0.1) on the shallow side, and the last open layer (porosity above 0.1) on the deep side.

At Styx Glacier, the shallowest depth where the running mean of total porosity with a 1 cm-thick window reaches below 0.1, is 48.1 m (Figs. 6a and 6b). It is approximately 4.3 m shallower than the LID of 52.4 m defined by the modelled firn air $\delta^{15}N\text{-}N_2$ profile. Meanwhile, the deepest point, where the running mean (with a 1 cm-thick window) exceeds 0.1, is at 63.7 m (Figs. 6a and 6c), which is shallower than the z_{COD} of 64.8 m defined by the deepest successful firn pumping depth. Although the LID and z_{COD} from the density data are different from those defined by firn air data, the thickness of LIZ from density data (between the two orange lines in Fig. 6a) is comparable to that from firn air analysis (between two blue lines in Fig. 6) (15.6 vs. 12.4 m). The offsets of the LIZ about 1-4 m between those from total porosity and the firn air measurement may be due to for example small calibration offsets in the density data set, the fact that actual critical porosity may be variable and depend on the study site, or on horizontal snow density variations and the horizontal extent of diffusion-impeding layers. The similarity in the LIZ thicknesses from the two methods support the idea that the

large variations of density can increase the LIZ thickness by shallowing LID and/or deepening the z_{COD}. The thick LIZ eventually permits storing old firn air at Styx (Table 1). Usually, the LIZ thickness increases with a snow accumulation rate (Witrant et al., 2012), presumably because at high accumulation sites density variability in the lock-in zone tends to increase (Horhold et al. 2011). Refrozen melt layers may also act as high density, diffusion-impeding layers allowing for older firn air to be sampled as observed in Devon Island (Witrant et al., 2012). We demonstrate here that the snow density variability is an important factor in determining the firn air age. We suggest that sites with higher density variations at the LIZ have a high possibility of a thick LIZ and therefore old firn air, even in warm, relatively high-precipitation coastal climates.

4 Discussions

To quantitatively compare density variability of Styx snow with those at other glacier sites, we may use the standard deviation of densities (σ_ρ) near the mean air-isolation density (Hörhold et al., 2011; Martinerie et al., 1992). The mean density at the mean air-isolation depth (ρ_{crit}) can be related to mean annual temperature (T in Kelvin) using the following equation, which is empirically obtained from air content measurements (Martinerie et al., 1992):

$$\rho_{\mathrm{crit}} = \left(\frac{1}{\rho_{ice}} + 7.6 \times 10^{-4} \times T - 0.057\right)^{-1} \quad (3),$$

where ρ_{ice} is the density of bubble-free pure ice.

Although this equation cannot provide exact ρ_{crit}, we can take advantage in estimating the density at LIZ without gas chemistry data (Hörhold et al., 2011). We note that Martinerie et al. (1994) suggested slightly different coefficients for the equation based on a different set of data; however, the results do not significantly change our conclusions. We also note that Bréant et al. (2018) used an equation relating ice density at LID to snow accumulation rate; however, we prefer to use the relation of temperature- ice density at LIZ by Martinerie et al. (1992) because the latter is more relevant to the ice density at LIZ. Using the Styx high-resolution X-ray density data at depth interval of 43.13-66.97 m, we calculated the standard deviation of densities (σ_ρ). For each σ_ρ, we used 1000 density data points (Fig. 7) as Hörhold et al. (2011) did for the other sites listed in Table 2. At Styx,

298 ρ_{crit} is 821.68 kg m^{-3} according to equation (4), and the standard deviation of densities at ρ_{crit} (σ_{ρ}, ρ_{crit}) is 19.33

299 $\pm$1.87 kg m^{-3}, which is greater than those in the other previously studied sites (Hörhold et al., 2011; Fig. 7,

300 Table 2). The high σ_{ρ}, ρ_{crit} at Styx likely facilitates the thick LIZ and old firn air.

301 A high-density (low-density) layer at surface may become a low-density (high-density) layer (Freitag et al.,
302 2004; Fujita et al., 2009) at density of 600-650 kg m^{-3}, which occurs at shallower depths than LIZ (Hörhold et
303 al., 2011). Thus, vertical snow layering at surface may not directly give information about density variability at
304 LIZ (Hörhold et al., 2011). However, conditions for snow layering at the surface still may give us clues on the
305 density variability at LIZ. The conditions may include redistribution of snow by wind and formation of wind
306 and/or radiation crusts (Martinerie et al., 1992; Hörhold et al., 2011). To test the possibility of seasonal causes,
307 we analyzed stable isotopes of surface snow ($\delta^{18}O$) because the surface $\delta^{18}O$ generally follows seasonal variation
308 (depleted in winter and enriched in summer). Figures 2e and 2f show the stable isotope profiles of snow ($\delta^{18}O$)
309 at Styx Glacier, which are apart by ~100 m; one is from a snow pit made in 2014 and the other is from the main
310 ice core drilled in 2014. The $\delta^{18}O$ profiles commonly show cycles with intervals of ~40 cm per year, given that
311 local maxima of $\delta^{18}O$ indicate summer, and minima winter layers. Meanwhile, the repetition of the density
312 layers has twenty cycles (high and low density layer pairs) in the top 180 cm depth at the snow pit (Fig. 2b).
313 Using a snow accumulation rate of ~40 cm y^{-1} in recent years, the density layers have 4~5 cycles y^{-1}, indicating
314 that the formation of snow density layers is mainly controlled by non-seasonal factors.

315 A blizzard occurred during the ice coring campaign in December of 2014. We observed that the blizzard
316 strongly reworked the surface snow. The Automatic Weather System (AWS) installed within 10 m from the
317 borehole site show that blizzard events (wind speed > 15 m s^{-1}) took place on December 29 in 2015, May 23,
318 June 26, August 17, and September 7 in 2016 (Fig. S1). The number of blizzard events in a year is similar to
319 the mean density layer cycle of 4~5 y^{-1}. Although Blizzards occur more frequently in winter, the frequency of 5
320 yr^{-1} is comparable to the number of the density layer cycles of 4~5 yr^{-1}. During the blizzard events, westerly
321 wind prevailed, and snow particles may have been redeposited with a sorted-size distribution (large grains in
322 the bottom and small grains on the top) similar to winnowing seen in sedimentary records (Sepp Kipfstuhl,
323 personal communication). Between the blizzards, the solar radiation and temperature gradient may have

facilitated the diagenesis of the snow layers (Alley, 1988; Fegyveresi et al., 2018). During the diagenesis processes, fine and coarse flake layers may form high-density and low-density layers, respectively. In summary, blizzard events may have played a major role in forming snow density layers

5 Conclusions and implications

About 93-year-old firn air (effective CO_2 age) was found at Styx Glacier, East Antarctica, located near the Ross Sea coast. This is of great scientific interest because such old firn air is commonly only found in the inland sites such as the South Pole and Megadunes. The thickness of Styx LIZ is relatively greater than those in other sites where snow accumulation and temperature are similar. The thicker LIZ made the Styx firn layer preserve old firn air because the age of stagnant firn air rapidly increases with depth in the LIZ as air exchange with the atmosphere has stopped. We hypothesized that the high snow density variations in the LIZ of Styx Glacier made the thick LIZ and old firn air. To test the hypothesis, we conducted high-resolution X-ray density measurements. We argue that the thick LIZ is related to the high density variations at Styx Glacier. We also examined why high snow density variability developed at Styx site. The effect of strong wind (e.g., blizzards) may facilitate the density layer formation. It is likely that old firn air (>55 years) can be found in areas where climatological conditions are favorable for high snow density variations at LIZ even when the sites are located near the coast. We may take advantage in sampling and transportation from the coastal sites, because logistics is easier for those sites. Theoretically, the oldest firn air should be available in a site that has both strong layering and a low accumulation rates. Older firn air, perhaps as old as 150 years, may still be found under such suitable conditions on the Antarctic continent.

Acknowledgements. We thank Jeff Severinghaus and Ross Beaudette at Scripps Institution of Oceanography for accurate $\delta^{15}N\text{-}N_2$ analysis, and Jacob Schwander at University of Bern for a kind advice in constructing the SNU firn air sampling device. We also thank Mauro Rubino and an anonymous reviewer for their constructive comments. This study was supported by Korea Polar Research Institute (PE 18040) and National Research Foundation of Korea (NRF-2018R1A2B3003256).

352 **References**

353 Alley, R. B.: Concerning the Deposition and Diagenesis of Strata in Polar Firn, Journal of Glaciology, 34, 283-
354 290, http://dx.doi.org/10.3189/s0022143000007024, 1988.

355 Aydin, M., Montzka, S.A., Battle, M.O., Williams, M.B., De Bruyn, W.J., Butler, J.H., Verhulst, K.R., Tatum,
356 C., Gun, B.K., Plotkin, D.A., Hall, B.D., and Saltzman, E.S.: Post-coring entrapment of modern air in some
357 shallow ice cores collected near the firn-ice transition: evidence from CFC-12 measurements in Antarctic
358 firn air and ice cores, Atmos. Chem. Phys., 10, 5135-5144, 2010.

359 Battle, M., Bender, M., Sowers, T., Tans, P.P., Butler, J.H., Elkins, J.W., Ellis, J.T., Conway, T., Zhang, N.,
360 Lang, P., and Clarke, A.D.: Atmospheric gas concentrations over the past century measured in air from firn
361 at the South Pole, Nature, 383, 231-235, 1996.

362 Battle, M. O., Severinghaus, J. P., Sofen, E. D., Plotkin, D., Orsi, A. J., Aydin, M., Montzka, S. A., Sowers, T.,
363 and Tans, P. P.: Controls on the movement and composition of firn air at the West Antarctic Ice Sheet Divide,
364 Atmospheric Chemistry and Physics Discussions, 11, 18633-18675, http://dx.doi.org/10.5194/acpd-11-
365 18633-2011, 2011.

366 Blunier, T. and Schwander, J.: Gas enclosure in ice: age difference and fractionation, in: Physics of Ice Core
367 Records, edited by: Hondoh, T., Hokkaido University Press, Sapporo, 307–326, 2000.

368 Bréant, C., Martinerie, P., Orsi, A., Arnaud, L., and Landais, A.: Modelling firn thickness evolution during the
369 last deglaciation: constraints on sensitivity to temperature and impurities, Clim. Past,13,833-853,
370 https://doi.org/10.5194/cp-13-833-2017,2017.

371 Buizert, C., Martinerie, P., Petrenko, V. V., Severinghaus, J. P., Trudinger, C. M., Witrant, E., Rosen, J. L., Orsi,
372 A. J., Rubino, M., Etheridge, D. M., Steele, L. P., Hogan, C., Laube, J. C., Sturges, W. T., Levchenko, V.
373 A., Smith, A. M., Levin, I., Conway, T. J., Dlugokencky, E. J., Lang, P. M., Kawamura, K., Jenk, T. M.,
374 White, J.W. C., Sowers, T., Schwander, J., and Blunier, T.: Gas transport in firn: multiple-tracer
375 characterisation and model intercomparison for NEEM, Northern Greenland, Atmos. Chem. Phys., 12,
376 4259–4277, doi:10.5194/acp-12-4259-2012, 2012a.

377 Buizert, C.: The influence of firn air transport processes and radiocarbon production on gas records from polar
378 firn and ice, PhD, Faculty of Science, University of Copenhagen, Denmark, Copenhagen, 175 pp., 2012b.

379 Buizert, C. and Severinghaus, J. P.: Dispersion in deep polar firn driven by synoptic-scale surface pressure

variability, The Cryosphere, 10, 2099–2111, https://doi.org/10.5194/tc-10-2099-2016, 2016.

Craig, H., Horibe, Y., and Sowers, T.: Gravitational separation of gases and isotopes in polar ice caps, Science, 242, 1675–1678, 1988.

Dlugokencky, E. J., Myers, R. C., Lang, P. M., Masarie, K. A., Crotwell, A. M., Thoning, K. W., Hall, B. D., Elkins, J. W., and Steele, L. P.: Conversion of NOAA atmospheric dry air CH4 mole fractions to a gravimetrically prepared standard scale, J. Geophys. Res., 110, D18306, https://doi.org/10.1029/2005JD006035, 2005.

Etheridge, D. M., Pearman, G. I., and Fraser, P. J.: Changes in tropospheric methane between 1841 and 1978 from a high accumulation-rate Antarctic ice core, Tellus B, 44, 282–294, doi:10.1034/j.1600-0889.1992.t01-3-00006.x, 1992.

Etheridge, D. M., Steele, L. P., Langenfelds, R. L., Francey, R. J., Barnola, J. M., and Morgan, V. I.: Natural and anthropogenic changes in atmospheric CO2 over the last 1000 years from air in Antarctic ice and firn, J. Geophys. Res., 101, 4115–4128, doi:10.1029/95jd03410, 1996.

Etheridge, D. M., Steele, L. P., Francey, R. J. and Langenfelds, R. L.: Atmospheric methane between 1000 A.D. and present: Evidence of anthropogenic emissions and climatic variability, Journal of Geophysical Research, 103(D13), 15979, doi:10.1029/98JD00923, 1998.

Fegyveresi, J. M., Alley, R. B., Muto, A., Orsi, A. J., and Spencer, M. K.: Surface formation, preservation, and history of low-porosity crusts at the WAIS Divide site, West Antarctica, The Cryosphere, 12, 325-341, http://dx.doi.org/10.5194/tc-12-325-2018, 2018.

Fourteau, K., Faïn, X., Martinerie, P., Landais, A., Ekaykin, A.A., Lipenkov, V.Y., Chapellaz, J., Analytical constraints on layered gas trapping and smoothing of atmospheric variability in ice under low-accumulation conditions, Clim. Past, 13, 1815–1830, 2017.

Freitag, J., Wilhelms, F., and Kipfstuhl, S.: Microstructure dependent densification of polar firn derived from X-ray microtomography, J. Glaciol., 50, 243–250, 2004.

Fujita, S., Okuyama, J., Hori, A., and Hondoh, T.: Metamorphism of stratified firn at dome fuji, antarctica: A mechanism for local insolation modulation of gas transport conditions during bubble close off, J. Geophys. Res., 114, F03023, doi:10.1029/2008JF001143, 2009.Goujon, C., Barnola, J. M., and Ritz, C.: Modeling the densification of polar firn including heat diffusion: Application to closeoff characteristics and gas

isotopic fractionation for Antarctica and Greenland sites, J. Geophys. Res.-Atmos, 108, 4792, doi:10.1029/2002JD003319, 2003.

Gregory, S. A., Albert, M. R., and Baker, I.: Impact of physical properties and accumulation rate on pore close-off in layered firn, The Cryosphere, 8, 91-105, http://dx.doi.org/10.5194/tc-8-91-2014, 2014.

Han, Y., Jun, S. J., Miyahara, M., Lee, H.-G., Ahn, J., Chung, J. W., Hur, S. D., and Hong, S. B.: Shallow ice-core drilling on Styx glacier, northern Victoria Land, Antarctica in the 2014-2015 summer, Journal of the Geological Society of Korea, 51, 343-355, 2015

Hörhold, M. W., Kipfstuhl, S., Wilhelms, F., Freitag, J., and Frenzel, A.: The densification of layered polar firn, Journal of Geophysical Research: Earth Surface, 116, http://dx.doi.org/10.1029/2009jf001630, 2011.

Hori, A., Tayuki, K., Narita, H., Hondoh, T., Fujita, S., Kameda, T., Shoji, H., Azuma, N., Kamiyama, K., Fujii, Y., Motoyama, H., and Watanabe, O.: A detailed density profile of the Dome Fuji (Antarctica) shallow ice core by X-ray transmission method, Annals of Glaciology, 29, 211-214, http://dx.doi.org/10.3189/172756499781821157, 1999.

Johnsen, S. J., Clausen, H. B., Cuffey, K. M., Hoffmann, G., Schwander, J., and Creyts, T.: Diffusion of stable isotopes in polar firn and ice: the isotope effect in firn diffusion, in: Physics of Ice Core Records, edited by: Hondoh, T., vol. 159, 121–140, Hokkaido University Press, Sapporo, Japan, 2000.

Kawamura, K., Severinghaus, J. P., Albert, M. R., Courville, Z. R., Fahnestock, M. A., Scambos, T., Shields, E., and Shuman, C. A.: Kinetic fractionation of gases by deep air convection in polar firn, Atmospheric Chemistry and Physics, 13, 11141-11155, http://dx.doi.org/10.5194/acp-13-11141-2013, 2013.

Landais, A., Barnola, J.M., Kawamura, K., Caillon, N., Delmotte, M., Van Ommen, T., Dreyfus, G., Jouzel, J., Masson-Delmotte, V., Minster, B., Freitag, J., Leuenberger, M., Schwander, J., Huber, C., Etheridge, D., and Morgan, V.: Firn-air δ15N in modern polar sites and glacial–interglacial ice: a model-data mismatch during glacial periods in Antarctica?, Quaternary Science Reviews, 25, 49-62, http://dx.doi.org/10.1016/j.quascirev.2005.06.007, 2006.

Laube, J. C., Hogan, C., Newland, M. J., Mani, F. S., Fraser, P. J., Brenninkmeijer, C. A. M., Martinerie, P., Oram, D. E., Röckmann, T., Schwander, J., Witrant, E., Mills, G. P., Reeves, C. E., and Sturges, W. T.: Distributions, long term trends and emissions of four perfluorocarbons in remote parts of the atmosphere and firn air, Atmos. Chem. Phys., 12(9), 4081-4090, 2012.

436 MacFarling Meure, C., Etheridge, D., Trudinger, C., Steele, P., Langenfelds, R., van Ommen, T., Smith, A., and
437 Elkins, J.: Law Dome CO2, CH4 and N2O ice core records extended to 2000 years BP, Geophys. Res. Lett.,
438 33, L14810, doi:10.1029/2006GL026152, 2006.
439 Martinerie, P., Raynaud, D., Etheridge, D. M., Barnola, J. M., and Mazaudier, D.: Physical and Climatic
440 Parameters which Influence the Air Content in Polar Ice, Earth Planet. Sc. Lett., 112, 1–13,
441 doi:10.1016/0012-821X(92)90002-D, 1992.
442 Martinerie, P., Lipenkov, V. Y., Raynaud, D., Chappellaz, J., Barkov, N. I., and Lorius, C.: Air content paleo
443 record in the Vostok ice core (Antarctica): A mixed record of climatic and glaciological parameters, J.
444 Geophys. Res., 99(D5), 10565– 10576, doi:10.1029/93JD03223, 1994.Mitchell, L. E., Buizert, C., Brook,
445 E. J., Breton, D. J., Fegyveresi, J., Baggenstos, D., Orsi, A., Severinghaus, J., Alley, R. B., Albert, M.,
446 Rhodes, R. H., McConnell, J. R., Sigl, M., Maselli, O., Gregory, S., and Ahn, J.: Observing and modeling
447 the influence of layering on bubble trapping in polar firn, J. Geophys. Res.-Atmos., 120, 2558–2574,
448 https://doi.org/10.1002/2014JD022766, 2015.
449 Petit, J. R., Jouzel, J., Raynnaud, D., Barkov, N. I., Barnola, J.-M., Basile, I., Bender, M., Chappellaz, J., Davis,
450 M., Delaygue, G., Delmotte, M., Kotlyakov, V. M., Legrand, M., Lipenkov, V. Y., Lorius, C., Pepin, L., Ritz,
451 C., Saltzman, E., and Stievenard, M.: Climate and atmospheric history of the past 420 000 years from the
452 Vostok ice core, Antarctica, Nature, 399, 429–436, 1999.
453 Proksch, M., Rutter, N., Fierz, C., and Schneebeli, M.: Intercomparison of snow density measurements: bias,
454 precision, and vertical resolution, The Cryosphere, 10, 371–384, doi:10.5194/tc-10-371-2016, 2016.
455 Rhodes, R. H., Fain, X., Stowasser, C., Blunier, T., Chappellaz, J., McConnell, J. R., Romanini, D., Mitchell, L.
456 E., and Brook, E. J.: Continuous methane measurements from a late Holocene Greenland ice core:
457 atmospheric and in-situ signals, Earth Planet. Sc. Lett., 368, 9–19, 2013.
458 Rhodes, R. H., Faïn, X., Brook, E. J., McConnell, J. R., Maselli, O. J., Sigl, M., Edwards, J., Buizert, C., Blunier,
459 T., Chappellaz, J., and Freitag, J.: Local artifacts in ice core methane records caused by layered bubble
460 trapping and in situ production: a multi-site investigation, Clim. Past, 12, 1061–1077, doi:10.5194/cp-12-
461 1061- 2016, 2016.
462 Rommelaere, V., Arnaud, L., and Barnola, J. M.: Reconstructing recent atmospheric trace gas concentrations
463 from polar firn and bubbly ice data by inverse methods, J. Geophys. Res.-Atmos., 102, 30069–30083,

464 doi:10.1029/97JD02653, 1997.
465 Rubino, M., Etheridge, D.M., Thornton, D.P. et al.: Revised records of atmospheric trace gases CO_2, CH_4,
466 N_2O, and $\delta^{13}C$-CO_2 over the last 2000 years from Law Dome, Antarctica, Earth Syst. Sci. Data, 11, 473–
467 492, 2019.
468 Schaller, C. F.., Freitag, J., and Eisen, O.: Critical porosity of gas enclosure in polar firn independent of climate,
469 Climate of the Past, 13, 1685-1693, http://dx.doi.org/10.5194/cp-13-1685-2017, 2017.
470 Schwander, J.: The transformation of snow to ice and the occlusion of gases, Environ. Rec. Glaciers Ice Sheets,
471 8, 53–67, 1989.
472 Schwander, J., Barnola, J.-M., Andrié, C., Leuenberger, M., Ludin, A., Raynaud, D., and Stauffer, B.: The age
473 of the air in the firn and the ice at Summit, Greenland, Journal of Geophysical Research: Atmospheres, 98,
474 2831-2838, http://dx.doi.org/10.1029/92jd02383, 1993.
475 Severinghaus, J. P., Grachev, A., and Battle, M.: Thermal fractionation of air in polar firn by seasonal
476 temperature gradients, Geochem. Geophy. Geosy., 2, 1048, doi:10.1029/2000GC000146, 2001.
477 Severinghaus, J. P., Albert, M. R., Courville, Z. R., Fahnestock, M. A., Kawamura, K., Montzka, S. A., Mühle,
478 J., Scambos, T. A., Shields, E., Shuman, C. A., Suwa, M., Tans, P., andWeiss, R. F.: Deep air convection in
479 the firn at a zero-accumulation site, central Antarctica, Earth Planet. Sc. Lett., 293, 359–367,
480 https://doi.org/10.1016/j.epsl.2010.03.003, 2010.
481 Sowers, T., Bender, M., Raynaud, D., and Korotkevich, Y. S.: Delta n-15 of n2 in air trapped in polar ice – a
482 tracer of gas-transport in the firn and a possible constraint on ice age-gas age-differences, J. Geophys. Res.-
483 Atmos., 97, 15683–15697, 1992.
484 Stauffer, B., Schwander, J., and Oeschger, H.: Enclosure of air during metamorphosis of dry firn to ice. Annals
485 of Glaciology, 6, 108-112. Doi:10.3189/1985AoG6-1-108-112, 1985.
486 Trudinger, C. M., Enting, I. G., Etheridge, D. M., Francey, R. J., Levchenko, V. A., Steele, L. P., Raynaud, D.,
487 and Arnaud, L.: Modeling air movement and bubble trapping in firn, J. Geophys. Res.-Atmos., 102, 6747–
488 6763, doi:10.1029/96JD03382, 1997.
489 Trudinger, C.M., Enting, I.G., Rayner, P.J., Etheridge, D.M., Buizert, C., Rubino, M., Krummel, P.B., and
490 Blunier, T.: How well do different tracers constrain the firn diffusivity profile?, Atmos. Chem. Phys. , 13,
491 1485-1510, https://doi.org/10.5194/acp13-1485-2013, 2013.

492 Witrant, E., Martinerie, P., Hogan, C., Laube, J. C., Kawamura, K., Capron, E., Montzka, S. A., Dlugokencky,
493 E. J., Etheridge, D., Blunier, T., and Sturges, W. T.: A new multi-gas constrained model of trace gas non-
494 homogeneous transport in firn: evaluation and behaviour at eleven polar sites, Atmos. Chem. Phys., 12,
495 11465–11483, doi:10.5194/acp-12-11465-2012, 2012.
496 Yang, J. W., Ahn, J., Brook, E. J., and Ryu, Y.: Atmospheric methane control mechanisms during the early
497 Holocene, Climate of the Past, 13, 1227-1242, http://dx.doi.org/10.5194/cp-13-1227-2017, 2017.
498 Yang, J. W., Han, Y., Orsi, A. J., Kim, S. J., Han, H., Ryu, Y., Jang, Y., Moon, J., Choi, T., Hur, S. D., and Ahn,
499 J.: Surface temperature in twentieth century at the Styx Glacier, northern Victoria Land, Antarctica, from
500 borehole thermometry. Geophysical Research Letters., 45, 9834-9842,
501 https://doi.org/10.1029/2018GL078770, 2018.
502 Yang, J. W.: Paleoclimate reconstructions from greenhouse gas and borehole temperature of polar ice cores, and
503 study on the origin of greenhouse gas in permafrost ice wedges, Ph.D. thesis, Department of Earth and
504 Environmental Sciences, Seoul National University, Seoul, 188 pp., 2019.
505

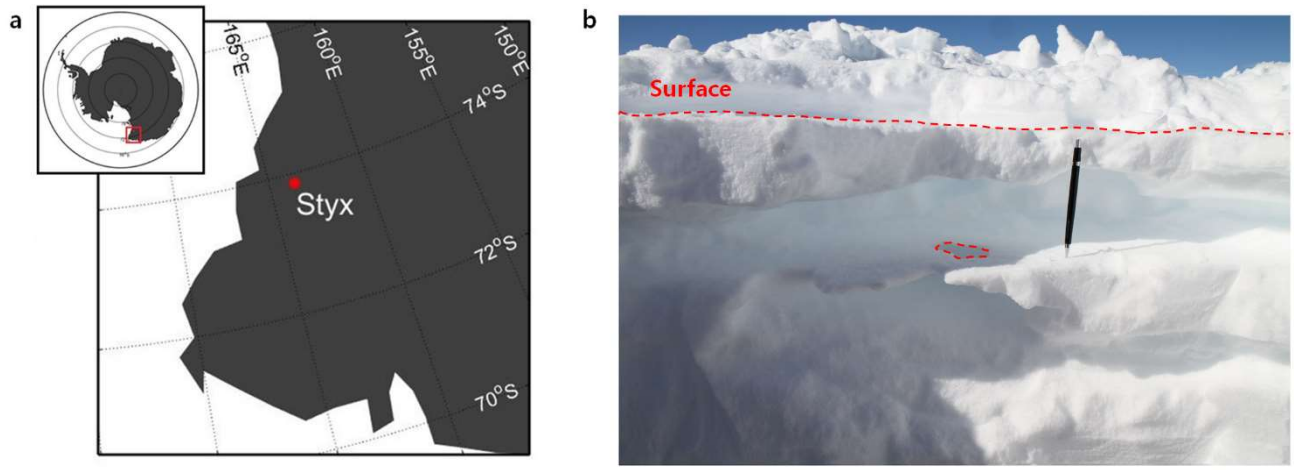

Figure 1. (a) Location map of study site, Styx Glacier, Antarctica and (b) a photo of surface snow density layers. The thickness of the snow density layers varies horizontally. The top boundaries of the high-density layers are sharp (horizontal red-dashed line). A hole on a high-density layer surface is indicated by a red-dashed circle. The length of the black sharp pencil in (b) is 14.3 cm.

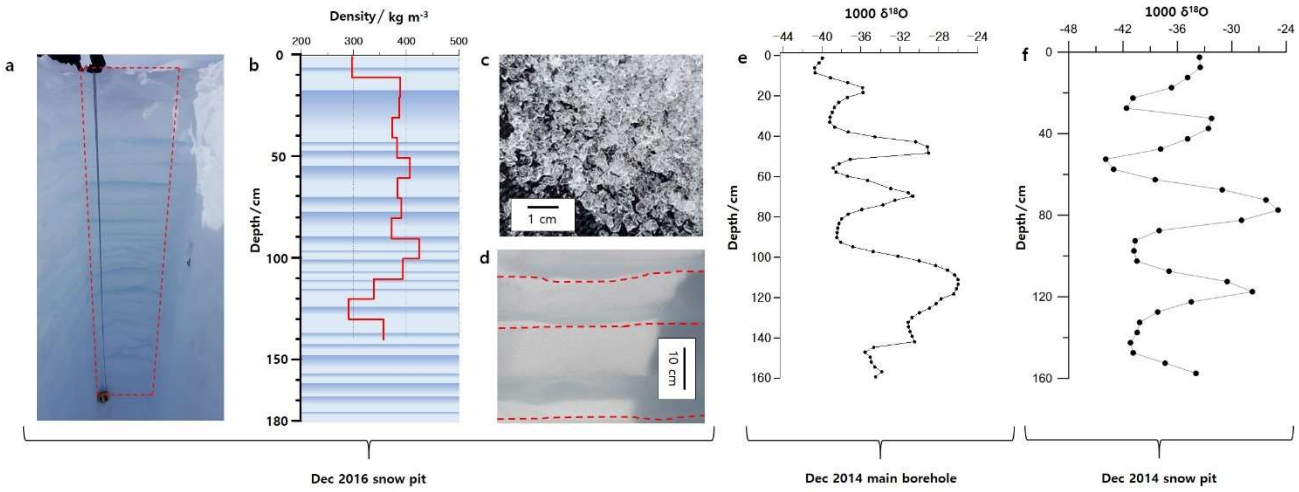

512

513 **Figure 2. Snow-pit photos at Styx Glacier. (a) The snow pit with dimensions of 280 × 65 × 220 cm (length**

514 **× width × height). (b) The illustration of qualitatively defined hard (dark blue) and soft (pale blue) layers**

515 **observed in the top 180-cm-depth interval. Progressive blue color changes indicate a gradual density**

516 **decrease with depth. Red line is a 10-cm-resolution density profile. (c) Coarse grains observed in a soft**

517 **layer. The grains were placed on a black glove. (d) Enlarged snow layers. Dashed red lines indicate top**

518 **boundaries of fine-grained hard layers. (e) and (f) Stable isotope ratio ($\delta^{18}O$) of snow profiles at the main**

519 **core and a snow pit 100 m away from the main ice core borehole, respectively.**

520 .

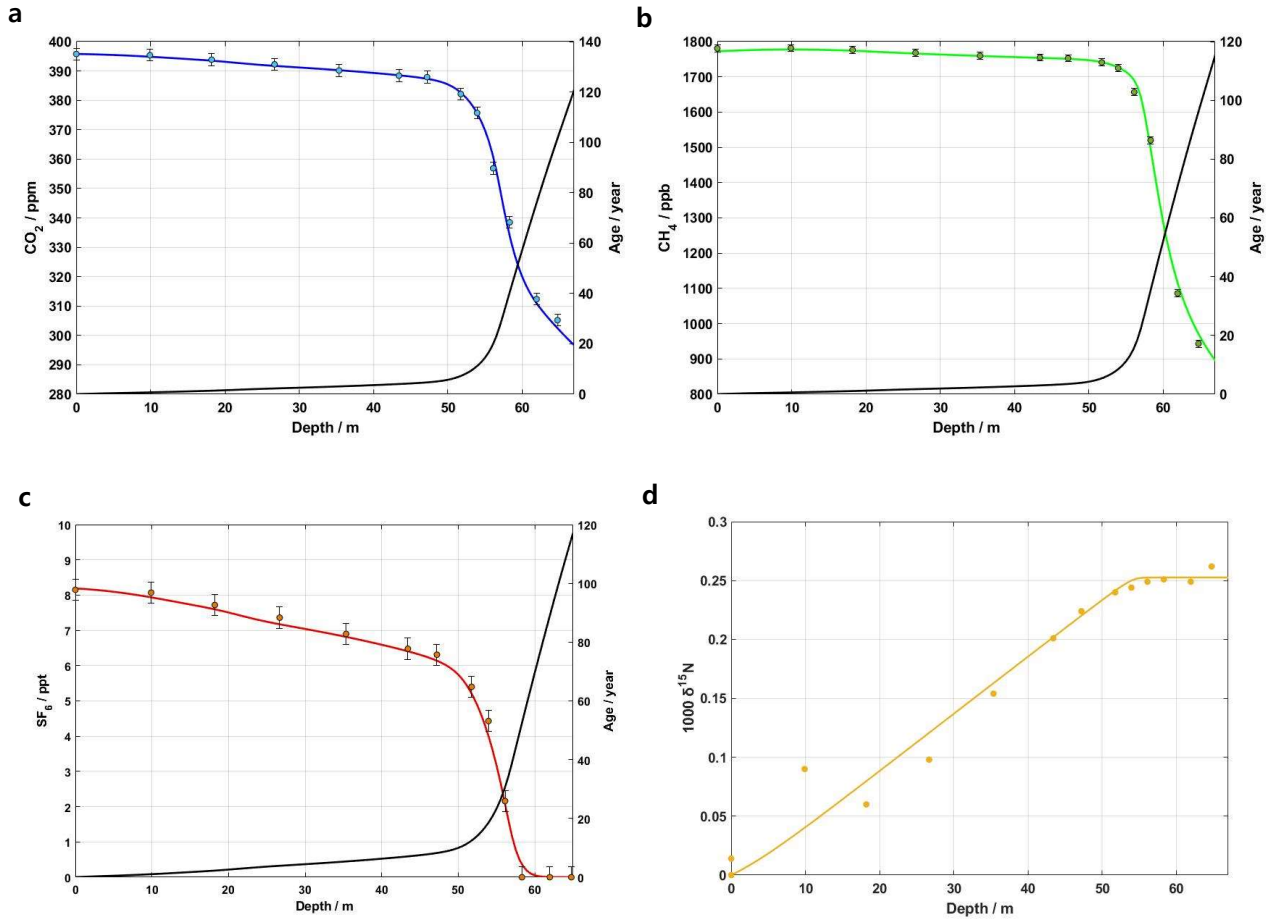

521

522 **Figure 3. CO_2, CH_4, SF_6 mole fractions and $\delta^{15}N$ of N_2 measurements (circles), and model results (solid**

523 **line) for the Styx firn air (air in open porosity). Black lines are modeled ages for the gas species.**

524

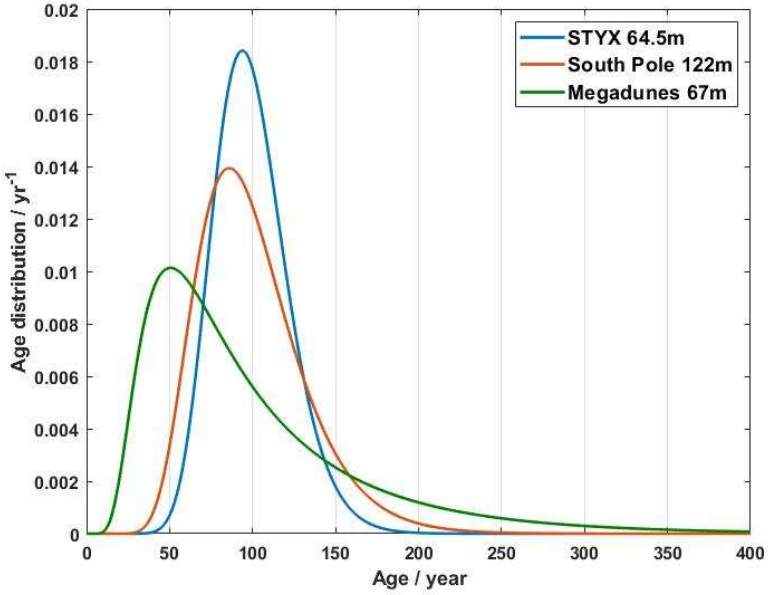

Figure 4. Comparison of model-simulated CO_2 age distributions at Styx (this study), South Pole (Battle et al., 1996), and Megadunes (Severinghaus et al., 2010).

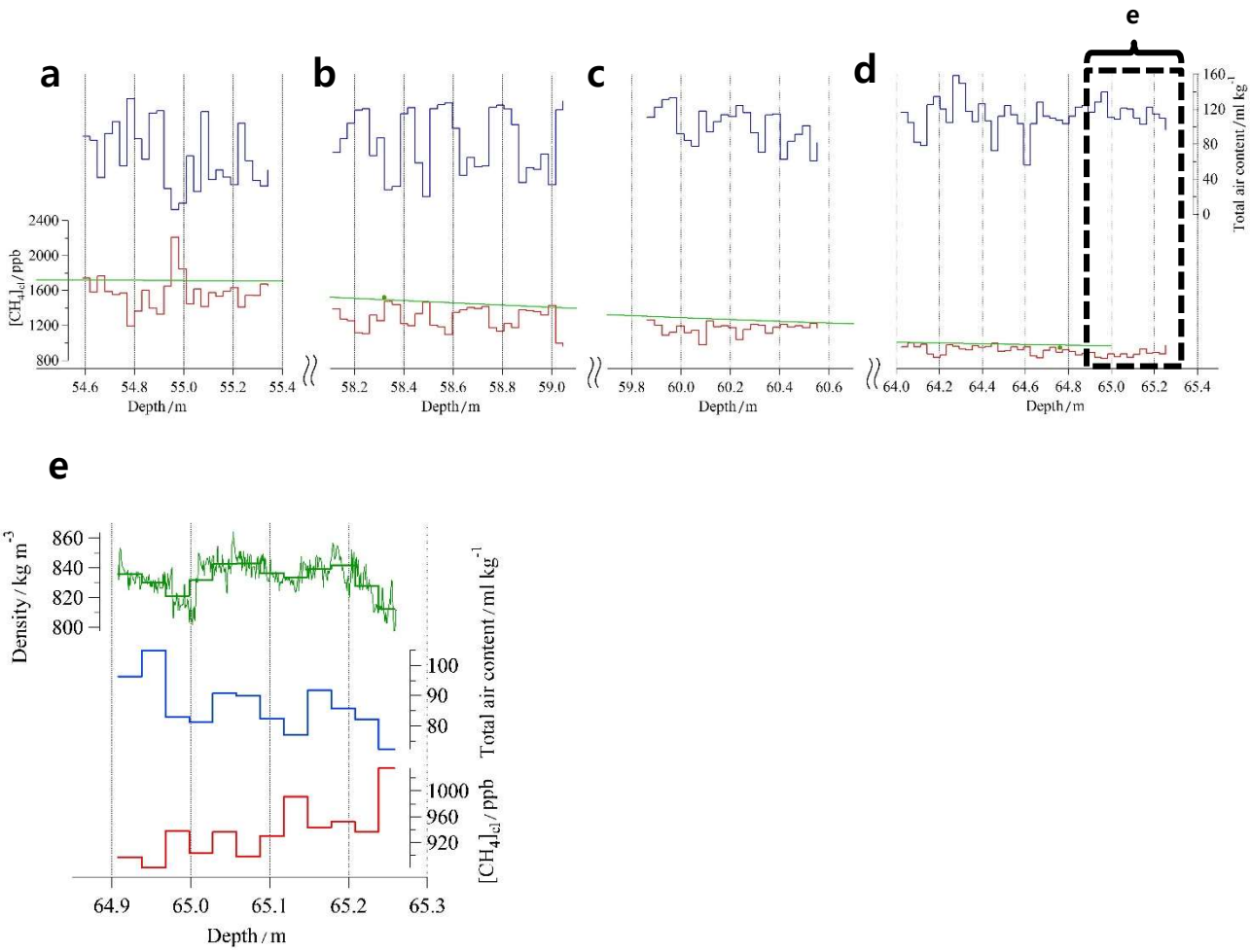

Figure 5. (a-d) CH_4 mole fraction in closed pores ($[CH_4]_{cl}$) (red line) and total air content (air volume per ice weight) (blue line) in the lock-in zone of Styx Glacier. (e) Comparison of density with $[CH_4]_{cl}$ and total air content near z_{COD}. A small dashed-box in (d) indicates the depth interval of Fig. 5e.

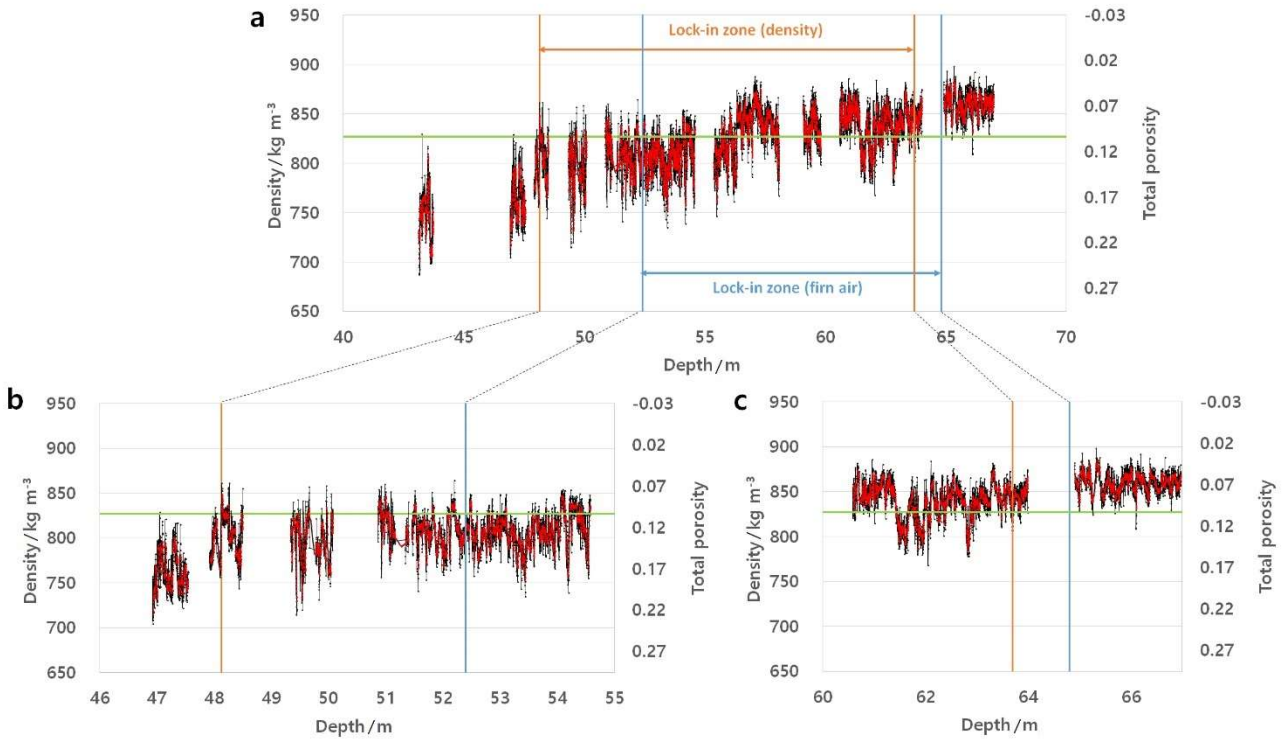

Figure 6. X-ray high-resolution density data obtained from the lock-in zone. (b) and (c) are enlarged portion of (a). Black lines show individual density data, while the red lines are 1-cm running means. Blue and orange lines represent the boundaries of the LIZ estimated from the gas compositions (between two vertical blue lines) and the critical porosity thresholds (between two orange vertical lines), respectively (see section 3.4).

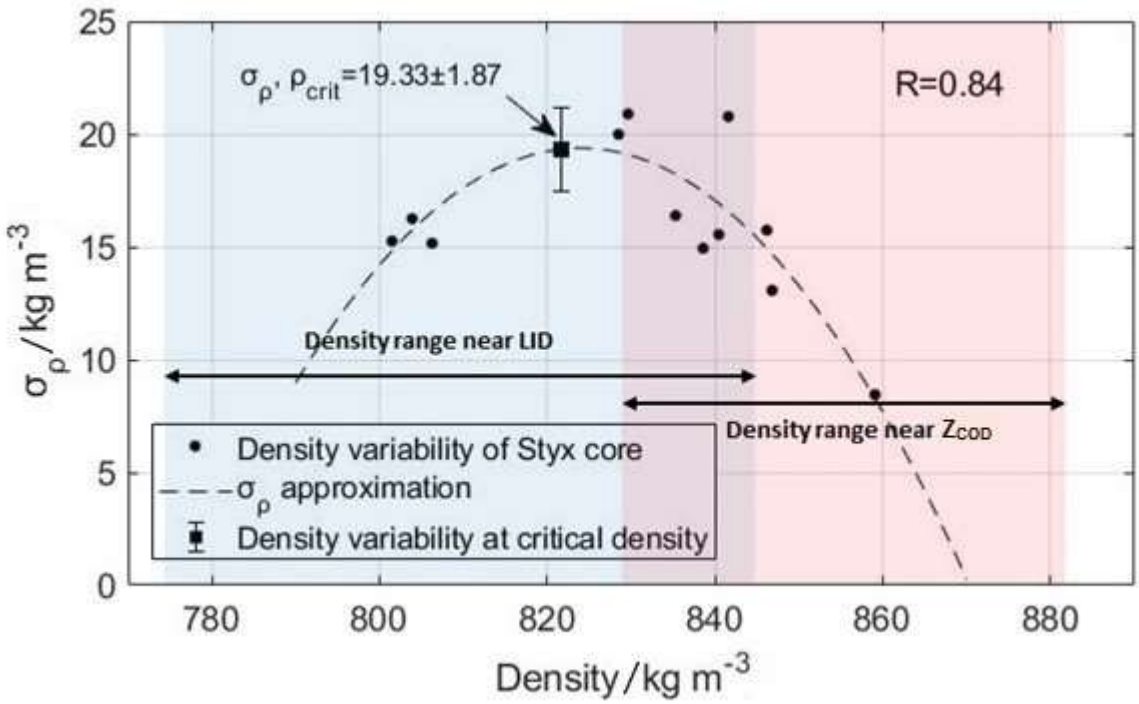

Figure 7. Density variability calculated from 1000 depth points and their average density. The standard deviation at the critical density (821.68 kg m^{-3}) calculated from the approximate second order polynomial (R = 0.84) is 19.33 ± 1.87 kg m^{-3}. The blue and red areas are the density ranges near the LID (52.38 - 52.48 m) and the z_{COD} (64.91 - 65.01 m), respectively.

Table 1. Glaciological characteristics of Styx Glacier and other firn air sampling sites.

Site	T (°C)	A (cm ice yr^{-1})	Effective CO_2 age (year)	LID (m)	COD (m)	LIZ thickness (m)	References
Styx	-31.7	10	93	52.4	64.8	12.4	This study, Yang et al. (2018)
Megadunes	-49	~0	129	64.5	68.5	4	Severinghaus et al. (2010)
South Pole	-51.0	8	91	115	125	10	Severinghaus et al. (2001)
Siple Dome	-25.4	13	59	49	58	9	Severinghaus et al. (2001)
Dome C	-54.5	2.7	33	97	100	3	Landais et al. (2006)
WAIS Divide	-31	22	39	~67	76.5	9.5	Battle et al. (2011)
NEEM	-28.9	22	50	63	78	15	Buizert et al. (2012a)
NGRIP	-31.1	19	45	67.5	78	11.5	Kawamura et al. (2006)
Summit	-32	23	26	70	80.8	10.8	Witrant et al. (2012)
DE-08	-19	120	13	71.8	88.5	16.8	Etheridge et al. (1996)

553 **Table 2. Comparison of standard deviation of density (σ_ρ) at critical density (ρ_{crit}). For data from all other**

554 **sites, except the Styx, refer to Hörhold et al. (2011).**

555

Campaign/Region	Core name	ρ_{crit} (kg m^{-3})	σ_ρ, ρ_{crit} (kg m^{-3})	T (°C)	A(cm ice yr^{-1})
Styx	Styx	821.68	19.33±1.87	-31.7	10
NGT	B16	819.27	12.26	-27	15.5
NGT	B18	820.81	12.81	-30	11.3
NGT	B21	820.81	12.91	-30	11.8
NGT	B26	820.85	13.23	-30.6	20
NGT	B29	821.32	10.50	-31.6	16.7
Berkner Island	B25	819.16	14.57	-27	15
DML	B31	827.00	10.27	-42	6.9
DML	B32	827.00	11.28	-42	6.7
DML	B36/37	827.50	8.12	-44.6	7.3
Pre-IPICS	B38	815.00	16.59	-18.1	136
Pre-IPICS	B39	814.91	17.11	-17.9	84
Pre-IPICS	DML95	815.51	13.42	-19.2	60
Pre-IPICS	DML97	816.07	10.03	-20.4	53
Dome C	EDC2	832.02	4.59	-53	2.7
WAIS Divide	WDC06A	820.81	10.35	-31	22

556